HHS Public Access

Author manuscript

Adv Mater. Author manuscript; available in PMC 2016 July 08.

Published in final edited form as:

Adv Mater. 2015 July 8; 27(26): 3901–3908. doi:10.1002/adma.201405660.

Levitational image cytometry with temporal resolution

S. Tasoglu[1], **J. Khoory**[2], **H. C. Tekin**[1], **C. Thomas**[3], **I. C. Ghiran**[2,*,a], and **U. Demirci**[1,*,a]

[1]Department of Radiology, Stanford School of Medicine, Canary Center at Stanford for Cancer Early Detection, Palo Alto, CA 94304

[2]Department of Medicine, Beth Israel Deaconess Medical Center, Harvard Medical School, Boston MA 02115

[3]Department of Pathology, Beth Israel Deaconess Medical Center, Harvard Medical School, Boston MA 02115

A wide variety of cellular processes, both physiological and pathological, are accompanied by transient or permanent changes in a cell's fundamental characteristics as a biological material (i) volumetric mass density or (ii) magnetic signature due to formation or quenching of intracellular paramagnetic reactive species such as, reactive oxygen species (ROS) and reactive nitrogen species (RNS). These events include cell-cycle stage [1], differentiation [2], cell-death (apoptosis/necrosis) [3], malignancy, disease state [4], activation, phagocytosis, *in vivo* and *ex vivo* cell aging (e.g., red blood cells), viral infection, and specific as well as non-specific responses to drugs. Therefore, reliable tools designed for high spatial resolution, real-time monitoring and quantification of magnetic signatures and volumetric mass densities of cells will help elucidate the intricate cellular mechanisms [5].

Hitherto, there have been attempts to measure the fundamental material properties of biological living materials with high precision such as the density of single living cells [6]. One such technology involves nanofabricated, suspended microchannel resonators that offers low throughput, and the necessity to use a sophisticated pump mechanism to transfer cells between fluids with different densities [5]. Other approaches include phase-shifting interferometry [7], digital holographic microscopy [8], quadriwave lateral shearing interferometry[9], and quantitative phase tomography [10]. Despite its success in quantifying cellular density, these technology has limitations in monitoring subtle morphological changes, manipulating cells or triggering and quantifying various cellular events without requiring sophisticated fabrication or components. Alternatively, magnetophoresis was used to separate cells based on their native magnetic properties, such as deoxygenated red blood cells (RBCs) from whole blood [11] and malaria-infected RBCs from healthy RBCs[12]. Magnetic repulsion was also used for label-free separation of cells spiked in magnetic solutions with respect to their size, elasticity and magnetic property[13]. However, these technologies are not capable to analyze various cell populations. Moreover, up until now,

*Corresponding Authors. ighiran@bidmc.harvard.edu, utkan@stanford.edu.
[a]These authors contributed equally.

COMPETING FINANCIAL INTERESTS

ST, IG, and UD declare competing financial interests in the form of a pending provisional patent (BWH Case No. 22697, filed on 02/25/14, "Real-Time, Multidimensional Functional Cellular Interrogation Using a Magnetic Levitation-Based Approach").

magnetic levitation has been used for analyses of densities and magnetic susceptibilities of individual, macroscopic objects and as a means effective in (i) separating foods[14], determining the fat content in milk, cheese, and peanut butter, (ii) comparing a variety of grains on the basis of their intrinsic densities, (iii) guiding self-assembly of objects[15, 16], (iv) characterizing forensic-related evidence [17], and noncontact orientation of objects[18]. Recently, a method has been demonstrated by using magnetic levitation approach to measure metal-amplified changes in the density of beads labeled with biomolecules[19]. By using gold nanoparticle-labeled biomolecules, and electroless deposition of gold or silver, change in the density of the beads were observed. These earlier magnetic levitation-based experiments were performed using large setups that had limited compatibility with microscopy[16, 20].

Here, we report a simple, yet powerful magnetic levitation-based device (Supplemental Fig. S1), fully compatible with upright or inverted fluorescence microscopes, which allows real-time, label-free separation, as well as high resolution monitoring of cell populations. While at current stage this technology does not aim to isolate or purify cell subpopulation, it offers rapid spatial separation of different cell populations based on their unique magnetic and density signatures, without the use of antibody-tagged magnetic beads, centrifugation steps, or the use of a specialized, continuous or discontinuous density gradient media. The levitation platform enables unique monitoring functional responses of cell populations (i) to a variety of stimuli, (ii) over time, and (iii) on a cell-by-cell basis.

Negative differences between the magnetic susceptibilities of suspending objects, χ_0, (e.g. a heterogeneous group of cells) and suspending medium (χ_{medium}) create a magnetic force field causing objects to be confined at different heights depending on the balance between buoyancy forces and magnetic forces (Fig. 1a). Until an object, e.g. a RBC suspended in a paramagnetic medium reaches the equilibrium height, a set of forces, i.e. fluidic drag, inertial, gravitational, and magnetic forces, continuously act on the object. As the object approaches equilibrium, its velocity, and thus drag and inertial forces become progressively smaller (Fig. 1b and Supplemental Fig. S2). In our experimental setup, a microcapillary tube with 1 mm × 1 mm square cross-section is placed between two permanent neodymium magnets (NdFeB) in a configuration where same poles facing each other. Using this configuration, magnetic forces exerting on the objects oppose the buoyancy forces, allowing objects to levitate at a height that depends on their density. To induce large magnetic forces on the objects, high grade (N52) NdFeB are chosen and they are placed closed to each other (1 mm). Two gold-coated mirrors are placed at each open side of the microcapillary at 45 degrees to create a device compatible with conventional microscopy systems for high resolution, spatiotemporal monitoring of cells during levitation (Fig. 1c). For higher resolution brightfield and fluorescence imaging (20×, 40× and 60×), we used a mirror-free setup coupled to a fluorescence upright microscope leveled on its side (see Methods). Due to the symmetric placement of the two magnets, the symmetric magnetic field strength distribution with respect to each axis reaching up to 0.4 T (Fig. 1d) was achieved. Hence, the suspended cells levitate at a position that depends on a) the location of minimum field strength and b) the ratios of the magnetic susceptibility and cellular density. To test our setup, we suspended RBCs isolated from a healthy donor in 40 mM gadolinium-based (Gd^+) paramagnetic medium (see Methods)[21]. The paramagnetic solution used for all

experiments presented here is currently employed for MRI investigations in humans. This medium is non-toxic, iso-osmolar at the concentration used for imaging, and fully compatible with human blood cells (see Supplemental Fig. S3). Following 10 minutes of magnetic confinement, RBCs stably levitated at a height of approximately 300 μm from the bottom magnet, forming a small, wall-less, blood stream-like assembly that can be easily imaged with high enough resolution to accurately quantify the basic parameters such as, shape, size, optical density, and multi-channel fluorescence of individual cells, for post-acquisition image cytometry (Fig. 1e).

Mass density distribution of human blood cells varies between 1.055 and 1.11 g/mL (Fig. 2a). Volumetric mass density defined as mass per unit volume is one of the most fundamental physical parameters that characterize a cell. Several cellular events such as differentiation, cell death (apoptosis/necrosis), malignancy, phagocytosis, and cell-age cause permanent or transient changes in cell volumetric mass density. We first assessed the cell-separation resolution of the setup, by magnetically focusing previously isolated and fluorescently labeled RBCs (red), polymorphonuclear leukocytes (PMNs), (green), and lymphocytes (blue) (Fig. 2b). Our results showed that cells suspended in 30mM Gd^+ solution form district density, and cell-type specific confinement bands populated by RBCs, PMNs and lymphocytes alone. Then, we investigated the effect of magnetic strength and density of the suspension solution on the focusing height of RBCs by progressively increasing the molarity of Gd^+ solution used for RBC suspension (Fig. 2c). We found that, as predicted by the formulas presented in supplemental data (Equations 11–12c), increases in the molarity of Gd^+, and thus magnetic susceptibility of the suspension media, and in a lesser degree of Gd^+ solution density (1.027 g/dL at 100 mM), caused a gradual increase in the focusing height of RBCs.

RBCs are formed in bone marrow by hematopoietic stem cells (HSCs), and circulate in average for 100–120 days before they are recycled by tissue macrophages. Circulating RBCs, through a complement-mediated process continuously release microparticles that progressively decrease their size, and surface-to-volume ratio, and increase their density[22]. To investigate if the sensitivity resolution of the setup was precise enough to separate young (1.09 g/mL) from old (1.11g/mL) RBCs based on their different volumetric mass densities, we levitated in a 30 mM Gd^+ solution, a mixture of fluorescently labeled young (green) and old (red) RBCs, which were isolated by Percoll® gradient (see Methods), using our published protocol[23]. RBCs, which were initially in random distribution in the microcapillary, started to focus at different levitation heights when exposed to magnetic field (snapshots of the time lapse recording are shown in Fig. 2d) (Supplementary Movie 1). Fluorescently labeled young and old RBCs at their respective equilibrium levitation heights are shown in Fig. 2e. Using the time-lapse recording of the levitation process, we evaluated analytically the specific equilibrium time function of focusing height of old and young RBCs (Fig. 2f). Briefly, equilibrium heights were measured from the bottom magnet for young and old RBCs and were found to be 0.156 mm and 0.092 mm, respectively. Density differences between each cell and suspension liquid were calculated using Supplemental Fig. S2 (plotted by Eq. 11). By substituting density differences into Eq. 14 and 15, equilibrium times were plotted (Fig. 2f). Next, we tested the capability of the setup to levitate gravitationally-sedimented cells. RBCs were loaded in the glass microcapillary tube, and

then placed on the bench for 15 minutes until all cells passively (gravitationally) sedimented along the bottom of the microcapillary. The microcapillary tube was then loaded in the magnetic levitation setup. Due to their relative diamagnetic properties compared to suspension liquid, cells started to move away from the magnet and levitate toward their density-dependent equilibrium point shown in Fig. 2g. We finally quantified the location of cells during magnetic focusing as a function of time using time-lapse microscopy (Fig. 2h).

PMNs are phagocytes, i.e. cells capable of sensing and responding to microorganism-specific danger signals followed by specific binding and internalization of foreign microorganisms or particles. Phagocytic events result in the formation of reactive oxygen species (ROS) and ROS-mediated activation of hydrolytic enzymes. Generation of ROS and reactive nitrogen species (RNS) will cause changes in the magnetic signature of phagocytes, whereas the dynamic interplay between the endocytic and exocytic processes during phagocytosis would directly impact the volumetric mass density of activated PMNs. To test the effect of cell activation on levitation height and cell morphology, we incubated freshly isolated PMNs with phorbol 12-myristate 13-acetate (PMA, 10 nM) for 10 minutes. As a control, PMNs were left in buffer for 10 minutes. Cells were then washed, fluorescently labeled, mixed together, and loaded into the magnetic levitation setup. Magnetic focusing revealed distinct differences between control and activated PMNs, both in terms of size, shape, optical density, as well as magnetic and mass density signatures (Fig. 3a). Activated PMNs generate intracellular paramagnetic ROS that actively reduces the difference between the magnetic susceptibilities of the cells and suspending medium. As a consequence, activated PMNs would be expected to “sink” compared to buffer-treated ones. However, our results show that the decrease in density promoted by cell activation [24] is more pronounced than the transient increase in magnetic properties and, as a result, the cells levitated to higher elevations than the control. The morphological differences between activated and normal PMNs were evaluated by measuring the roundness of cells, defined as $perimeter^2/(4 \cdot \pi \cdot area)$. Calculated roundness values indicated significant difference between PMA-activated and buffer-treated PMNs (Fig. 3c). The same samples were simultaneously examined by flow cytometry for changes in forward and side-scatter properties of PMNs associated with PMA activation (Fig. 3d). When compared to flow cytometry, magnetic levitation allows direct visualization of cells, as well as increased shape and size-detection sensitivity and resolution, while simultaneously providing real-time density measurements on a cell-by-cell basis. To further understand the effect of intracellular ROS on the final position of levitating cells, we used cell permeable glutathione (GSH), a known ROS scavenger. Our results showed that GSH-treated PMNs equilibrated slightly below the resting PMNs, whereas activated, low density PMNs were focused as expected, above these two groups (Fig. 3e). These results support the hypothesis that ROS potentially changes the magnetic susceptibilities of the cells to an extent in which the levitation heights differ. To test the density resolution of the setup, we next levitated a mixture of PMNs (PMN), lymphocytes (L) and platelets (P). High magnification imaging of the resting PMNs revealed that, while most of the cells were non-activated, a few (Fig. 3f, arrow) showed early signs of activation, through both shape changes and height positions, indicative of lower cell density. In addition, contaminating eosinophils were positioned at the bottom of the PMN column, consistent with their density being equal to or greater than that of the densest PMNs (see

Fig. 2a). Two hours after continuous levitation, PMNs underwent self-activation [25] followed by integrin-mediated homo-typical aggregation (Fig. 3g). Of note, some of the PMN clusters also displayed a lower position compared to non-activated PMNs, suggesting that intracellular, paramagnetic ROS species formed during activation also influenced the confinement height of the cells. Next, we studied the relative density changes during human PMN phagocytosis by incubating freshly isolated PMNs with fluorescently labeled *Salmonella montevideo* (Fig. 3h). Our results show that phagocytic PMNs have significantly decreased density although there was no clear relationship between the numbers of *Salmonella* ingested (shown as red, in Fig. 3h) and the confinement height of the PMNs. Our experiments are also showed that labeling the cells with fluorescent dyes did not alter the levitation height of cells (Supplemental Fig. S4).

To demonstrate the wide applicability of this magnetic levitation-based approach over different cell types, we used circulating cancer cells, and sickled RBCs. Metastasis is a process responsible for spreading malignant cells from the primary site to another, non-adjacent site. When malignant cells break away from a tumor, they migrate to other areas of the body through the bloodstream or the lymph system, becoming circulating tumor cells (CTC). We prepared a heterogeneous group of cells by spiking normal blood with breast cancer cells (CTC) (Fig. 4a) pre-stained with the cell permeable, DNA-specific dye Hoechst 33342. The cell mixture was then magnetically focused for 15 minutes in a 20 mM Gd^{+} solution that allowed levitation only of PMNs and lymphocytes (L), but not that of RBCs. CTCs were readily identified (nucleus stained blue in Fig. 4b, and overlay in Fig. 4c) from the multi-cell suspension being confined close to the center of the microcapillary tube, tens to hundreds of micrometers away from lymphocytes and PMNs respectively. Although we used a significantly larger number of tumor cells that those that would normally be found in blood of a patient, the aim of the experiment was to test the device to spatially distinguish cells blood cells from cells with high genetic and morphological variability such as tumor cell. We also tested the ability of magnetic levitation to provide a binary answer, critical for rapid tests aimed at point of care (POC)-type settings. We levitated and recorded the responses of RBCs isolated from a healthy donor, and a patient homozygous (SS) for sickle cell disease in the absence (Supplemental Fig. S5) or presence of 10 mM sodium metabisulfite [26]. Our results show that while sodium metabisulfite does not alter the density of healthy RBCs (Fig. 4d), RBCs from SS patients fail to maintain their initial densities, rendering a subpopulation of sickle RBCs, significantly denser (Fig. 4e), displaying a distribution pattern that is both unique, as well as easily quantifiable with standard image analysis methods (Supplemental Fig. S6).

We have demonstrated the versatility of the magnetic levitation platform that allows spatial separation and activation of cells, as well as monitoring and quantifying of various morphological attributes, specific cellular activities and agonist responses in real-time. The strategy presented here allows also the examination of temporal responses of cells (Supplementary Fig. S7) that could potentially provide extensive morphological and functional mapping capabilities over time on a cell-by-cell basis for a given population. This device separated cells in a 1 mm capillary, so the cells are spatially enriched in a 3-D space. The advantages of the system include (i) simple workflow, (ii) lack of sophisticated micro/nano-fabrication components (iii) disposable designs with the possibility for autoclaveable

reusable modules, and (iv) multidimensional, real-time investigation of dynamic cell:cell communications such as antigen-presenting cell:T cell and platelet:monocyte interactions [27].

Several flow-based microfluidic devices have been developed for isolating and purifying cells in the last decade for numerous applications. Here, we did not aim to isolate or purify cell subpopulations. While flow-based microfluidic approaches impart with high throughput, such approaches have to waive a simple yet crucial capability, i.e. real-time spatial and morphological tracking of cell subpopulations and their responses to several factors e.g. ROS formation or phagocytic events over large time durations. The presented approach here offers rapid spatial separation of different cell populations based on their magnetic signatures and densities without the use of antibody-tagged magnetic beads, centrifugation or the use of a specialized, continuous or discontinuous density gradient media.

The magnetic levitation device offers numerous biotechnology applications as well as a platform to study and monitor several fundamental cellular behavior. It provides unique capabilities for cell biology research where cell densities matter, and can reflect various processes such as cell-cycle, phagocytosis, apoptosis, and differentiation. This system is also sensitive to magnetic susceptibilities of cells, and can thus be used for analysis of hemoglobin degradation within the RBCs (e.g. stored blood and sickle cells). The capability of monitoring several cellular activities can be also significant for drug discovery, toxicity testing, and single cell testing. Real-time monitoring of levitating cells, followed by protein and nucleic acid analyses, will potentially open avenues for research in unique signaling mechanisms present only during low gravity conditions.

Simplicity, small size-scale and flexibility of the design can potentially make the system compatible with mobile devices for telemedicine and use in resource poor settings for screening and diagnostics of malaria-infected red blood cells and sickle cells. This strategy does not require antibodies, advanced microscopy instrumentations or techniques for reliable diagnosis, nor the presence of microscopy specialists. The presented magnetic-levitation based approach provides a broadly applicable tool for high resolution, real-time cell biology research, as well as for binary disease screening and diagnostics suitable for point-of-care settings.

METHODS

Antibodies and Reagents

Hoecsht 33342 (H1399, Molecular Probes, Eugene, OR); Hank’s Balanced Salt Solution (14025-092), Cell Mask Deep Red plasma membrane stain (C10046), Cell Tracker Green, CMFDA (C-7025), NPE-caged ATP (A-1048, Life Technologies, Grand Island, NY); Ficoll® (17-5442-03), Percoll® (17-0891-01, GE Healthcare, Pittsburgh, PA); citrate 4% w/v (S5770), Dextran T500 (31392), Glutathione reduced ethyl ester (GSH-ME, G1404), Sodium metabisulfite (S9000), Sodium Chloride (S5886, Sigma, St. Louis, MI); Phorbol 12-myristate 13-acetate (PMA, 1201, Tocris, Bristol, United Kingdom); VitroTubes™ Square Capillary Microcells, Borosilicate Glass (8100, Vitrocom, Mountain Glass, NJ);

Gadolinium-based (Gd^{+}) paramagnetic medium Prohance® (Bracco Diagnostics, Princeton, NJ); Critoseal™ (Fisher Scientific, Pittsburgh, PA).

Magnetic Levitation of Cells

Cells were resuspended in 200 μL of 40 mM Gadolinium solution unless otherwise noted, all blood cells used were isolated and purified before being diluted (see methods on PBMC, PMN, and RBC isolations in the Supplementary Information) into the 1.0 × 1.0 mm square microcapillary tubes(wall thickness 0.2 mm) by superficial tension action. Critoseal™ was inserted into either end of the microcapillary to prevent cells from drifting during analysis. The capillary was then loaded into a slot between the magnets and cells were imaged using either QImaging Emc^2 EMCCD camera on an Olympus BX62 microscope or an Qimaging EXi CCD camera on a Zeiss Axioscope microscope. For high-resolution images, we placed a fluorescence microscope leveled on its side perfectly horizontal, and used a mirror-free magnetic levitation setup. The images were analyzed with Slidebook 5.5. (3i, Denver, CO), ImageProPlus 7 (Media Cybernetics, Rockville, MD), and iVison 4.7 (Biovision, Exton PA).

Supplementary Material

Refer to Web version on PubMed Central for supplementary material.

Acknowledgments

UD acknowledges that this material is based in part upon work supported by the NSF CAREER Award Number 1150733, NIH R01EB015776-01A1 and NIH R21HL112114. IG acknowledges that this material is based in part upon work supported by the NIH R01 HL096795, NIH R21TW009915, and Bill and Melinda Gates Foundation award OPP1032683. UD is a founder of, and has an equity interest in: **(i)** DxNow Inc., a company that is developing microfluidic and imaging technologies for point-of-care diagnostic solutions, and **(ii)** Koek Biotech, a company that is developing microfluidic IVF technologies for clinical solutions. UD's interests were reviewed and are managed by the Brigham and Women's Hospital and Partners HealthCare in accordance with their conflict of interest policies. We thank Dr. Peter Weller and Anne-Nicholson Weller for reading the manuscript and helpful comments.

References

1. Wolff DA, Pertoft H. Journal of Cell Biology. 1972; 55:579. [PubMed: 4571230]
2. Maric D, Maric I, Barker JL. Methods-a Companion to Methods in Enzymology. 1998; 16:247.
3. Martin SJ, Bradley JG, Cotter TG. Clinical and Experimental Immunology. 1990; 79:448. [PubMed: 2317949] Wyllie AH, Morris RG. American Journal of Pathology. 1982; 109:78. [PubMed: 6289672]
4. Mrema JE, Campbell GH, Miranda R, Jaramillo AL, Rieckmann KH. Bulletin of the World Health Organization. 1979; 57:133. [PubMed: 371850] Rodgers GP, Schechter AN, Noguchi CT. Journal of Laboratory and Clinical Medicine. 1985; 106:30. [PubMed: 4009021]
5. Grover WH, Bryan AK, Diez-Silva M, Suresh S, Higgins JM, Manalis SR. Proceedings of the National Academy of Sciences of the United States of America. 2011; 108:10992. [PubMed: 21690360] Bryan AK, Goranov A, Amon A, Manalis SR. Proceedings of the National Academy of Sciences. 2009Bryan AK, Hecht VC, Shen W, Payer K, Grover WH, Manalis SR. Lab on a Chip. 2014; 14:569. [PubMed: 24296901]
6. Son S, Tzur A, Weng Y, Jorgensen P, Kim J, Kirschner MW, Manalis SR. Nat Meth. 2012; 9:910.Park K, Millet LJ, Kim N, Li H, Jin X, Popescu G, Aluru NR, Hsia KJ, Bashir R. Proceedings of the National Academy of Sciences. 2010; 107:20691.Godin M, Delgado FF, Son S, Grover WH, Bryan AK, Tzur A, Jorgensen P, Payer K, Grossman AD, Kirschner MW, Manalis SR. Nat Meth. 2010; 7:387.Zangle TA, Teitell MA. Nat Meth. 2014; 11:1221.

7. Reed J, Chun J, Zangle Thomas A, Kalim S, Hong Jason S, Pefley Sarah E, Zheng X, Gimzewski James K, Teitell Michael A. Biophysical Journal. 101:1025. [PubMed: 21889438]
8. Mir M, Wang Z, Shen Z, Bednarz M, Bashir R, Golding I, Prasanth SG, Popescu G. Proceedings of the National Academy of Sciences. 2011; 108:13124.
9. Bon P, Maucort G, Wattellier B, Monneret S. Opt Express. 2009; 17:13080. [PubMed: 19654713] Bon P, Savatier J, Merlin M, Wattellier B, Monneret S. BIOMEDO. 2012; 17:0760041.
10. Cotte Y, Toy F, Jourdain P, Pavillon N, Boss D, Magistretti P, Marquet P, Depeursinge C. Nat Photon. 2013; 7:113.
11. Melville D. Nature. 1975; 255:706. [PubMed: 1134566] Han K-H, Bruno Frazier A. Journal of Applied Physics. 2004; 96:5797.Furlani EP. Journal of Physics D: Applied Physics. 2007; 40:1313.
12. Nam J, Huang H, Lim H, Lim C, Shin S. Analytical Chemistry. 2013; 85:7316. [PubMed: 23815099]
13. Kose AR, Koser H. Lab on a chip. 2012; 12:190. [PubMed: 22076536] Kose AR, Fischer B, Mao L, Koser H. Proceedings of the National Academy of Sciences of the United States of America. 2009; 106:21478. [PubMed: 19995975] Shen F, Hwang H, Hahn YK, Park J-K. Analytical Chemistry. 2012; 84:3075. [PubMed: 22380761] Erb RM, Yellen BB. Magnetics IEEE Transactions on. 2006; 42:3554.
14. Mirica KA, Phillips ST, Mace CR, Whitesides GM. Journal of Agricultural and Food Chemistry. 2010; 58:6565. [PubMed: 20465289]
15. Mirica KA, Ilievski F, Ellerbee AK, Shevkoplyas SS, Whitesides GM. Advanced Materials. 2011; 23:4134. [PubMed: 21830239] Tasoglu S, Kavaz D, Gurkan UA, Guven S, Chen P, Zheng R, Demirci U. Advanced Materials. 2013; 25:1137. [PubMed: 23288557]
16. Tasoglu S, Yu CH, Gungordu HI, Guven S, Vural T, Demirci U. Nat Commun. 2014:5.
17. Lockett MR, Mirica KA, Mace CR, Blackledge RD, Whitesides GM. Journal of Forensic Sciences. 2013; 58:40. [PubMed: 22804094]
18. Subramaniam AB, Yang D, Yu HD, Nemiroski A, Tricard S, Ellerbee AK, Soh S, Whitesides GM. Proceedings of the National Academy of Sciences. 2014; 111:12980.
19. Subramaniam AB, Gonidec M, Shapiro ND, Kresse KM, Whitesides GM. Lab on a Chip. 2015
20. Atkinson MBJ, Bwambok DK, Chen J, Chopade PD, Thuo MM, Mace CR, Mirica KA, Kumar AA, Myerson AS, Whitesides GM. Angewandte Chemie International Edition. 2013; 52:10208.Bwambok DK, Thuo MM, Atkinson MBJ, Mirica KA, Shapiro ND, Whitesides GM. Anal Chem. 2013; 85:8442. [PubMed: 23972068] Shapiro ND, Mirica KA, Soh S, Phillips ST, Taran O, Mace CR, Shevkoplyas SS, Whitesides GM. Journal of the American Chemical Society. 2012; 134:5637. [PubMed: 22364170] Shapiro ND, Soh S, Mirica KA, Whitesides GM. Anal Chem. 2012; 84:6166. [PubMed: 22686324]
21. Winkleman A, Gudiksen KL, Ryan D, Whitesides GM, Greenfield D, Prentiss M. Applied Physics Letters. 2004; 85:2411.
22. Linderkamp O, Friederichs E, Boehler T, Ludwig A. British Journal of Haematology. 1993; 83:125. [PubMed: 8435319]
23. Costa M, Ghiran I, Peng CK, Nicholson-Weller A, Goldberger AL. Physical Review E. 2008:78.
24. Pember S, Barnes K, Brandt S, Kinkade JJ. Blood. 1983; 61:1105. [PubMed: 6839018]
25. Fearon DT, Collins LA. Journal of Immunology. 1983; 130:370.
26. Asakura T, Mayberry J. Journal of Laboratory and Clinical Medicine. 1984; 104:987. [PubMed: 6502005]
27. Freedman JE, Loscalzo J. Circulation. 2002; 105:2130. [PubMed: 11994242] Dustin ML. Seminars in Immunology. 2005; 17:400. [PubMed: 16266811]

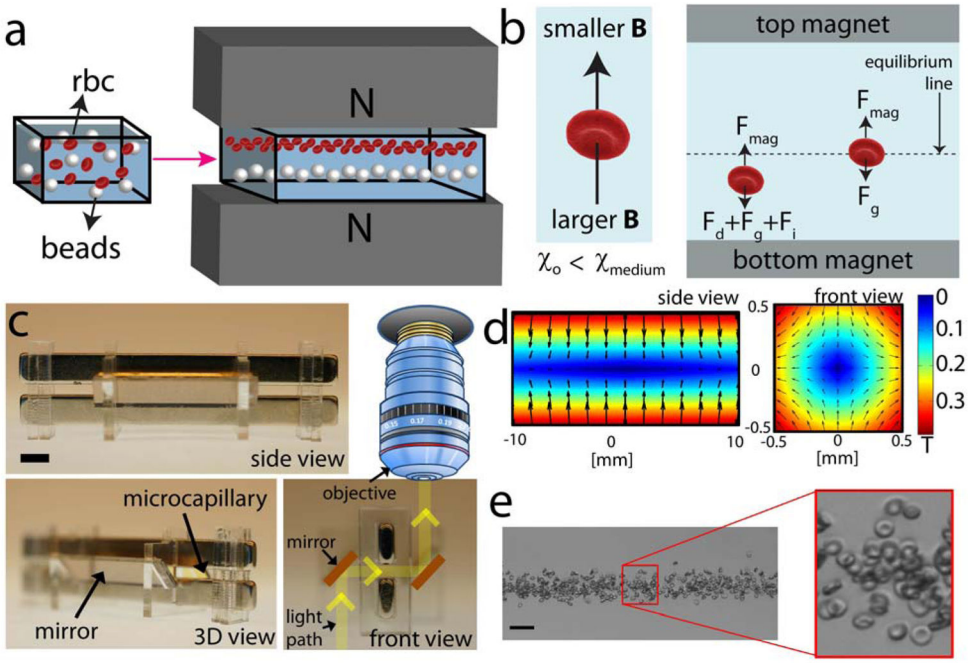

Figure 1. Magnetic levitation-based device for static separation, cytometry and functional interrogation of cells

(a) Schematic of the magnetic levitation and cell manipulation in a magnetic field. **(b)** Negative difference between the magnetic susceptibilities of an object (χ_0) and suspending medium (χ_{medium}) causes the object to move away from larger magnetic field strength site to lower magnetic field strength. Until the object reaches the equilibrium, fluidic drag (F_d), inertial (F_i), buoyancy (F_g), and magnetic forces (F_m) act on the object. As the object gets closer to the equilibrium, its migration velocity, and thus drug and inertial forces, become smaller. **(c)** Front, 3D, and side views of the magnetic levitation setup. A capillary with 1 mm × 1 mm square cross-section is placed between two permanent neodymium magnets (NdFeB) in a configuration where same poles facing each other. Scale bar is 3 mm. **(d)** Controlling the position and orientation of objects with magnetic field gradients. Contour plot of the magnetic field for two magnets with same poles facing each other. The magnitude of the magnetic field is constrained between 0 T and 0.4 T. More information on modeling is given in Supplementary Information. **(e)** Confinement of RBCs in 50 mM Gd^+ solution. Scale bar is 40 μm.

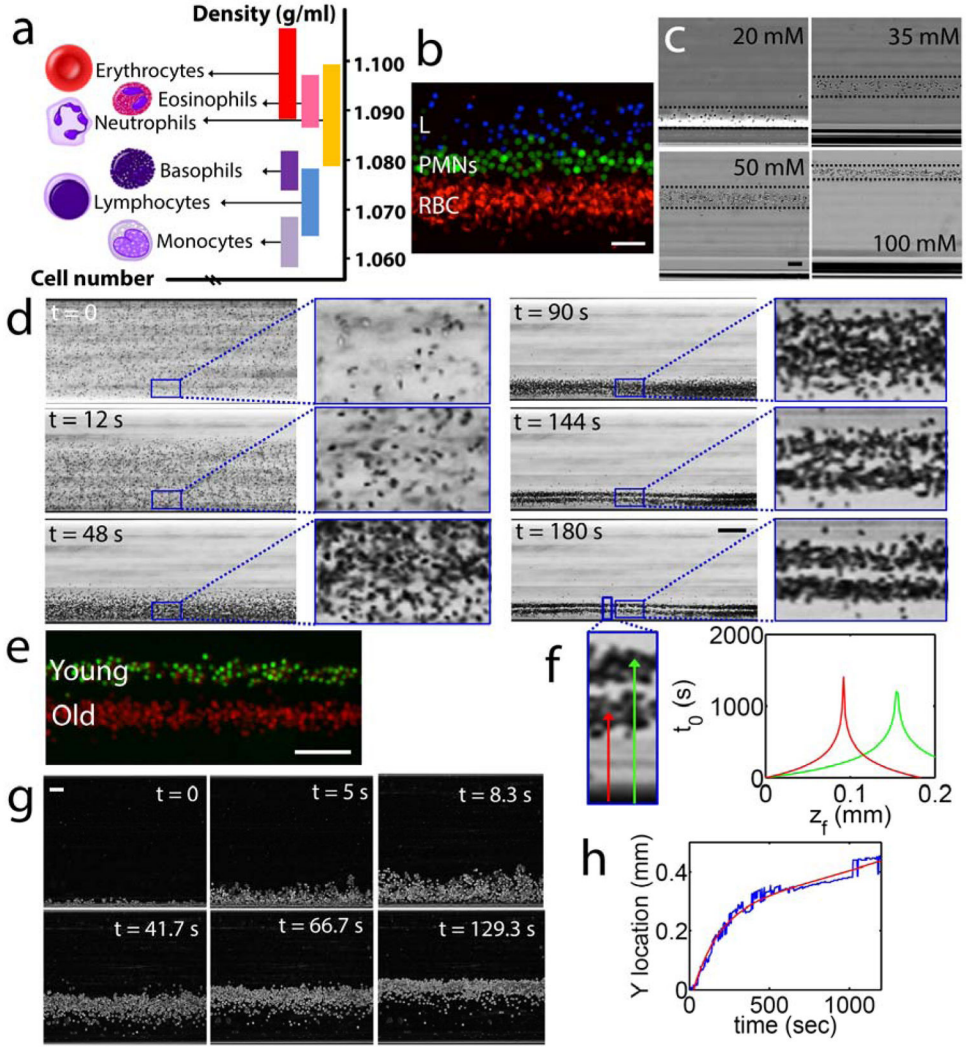

Figure 2. Characterization of cell separation using magnetic levitation

(a) Density histogram of monocytes, lymphocytes, basophils, PMNs, eosinophils, and RBCs. **(b)** Magnetically-driven, density-based separation of fluorescently-labeled blood cells. Freshly purified RBCs (RBCs, labeled red), PMNs (PMNs, labeled green), and lymphocytes (L, labeled blue) were mixed and magnetically confined for 15 minutes in 30 mM Gd^+ solution. Scale bar is 40 μm. **(c)** Levitation of RBCs at different molarities of suspending Gd^+ solution, from left to right: 20, 35, 50, and 100 mM Gd^+ solution. Scale bar is 40 μm. **(d)** Separation of young and old RBCs by age (Supplementary Movie 1). Time-lapse images showing the density separation of a mixed population of purified young and old RBCs. Scale bar is 160 μm. **(e)** Fluorescently labeled young (green) and old (red) RBCs at their equilibrium levitation height. Scale bar is 100 μm. **(f)** Analytical equilibration time as a function of equilibration height of old and young RBCs. **(g)** True magnetic levitation in whole blood (diluted 1:1000). Sedimented RBCs were loaded into the magnetic levitation device and cells imaged for 20 minutes. Scale bar is 40 μm. **(h)** Time-dependent location of RBCs levitating from bottom surface of microcapillary toward their equilibration point.

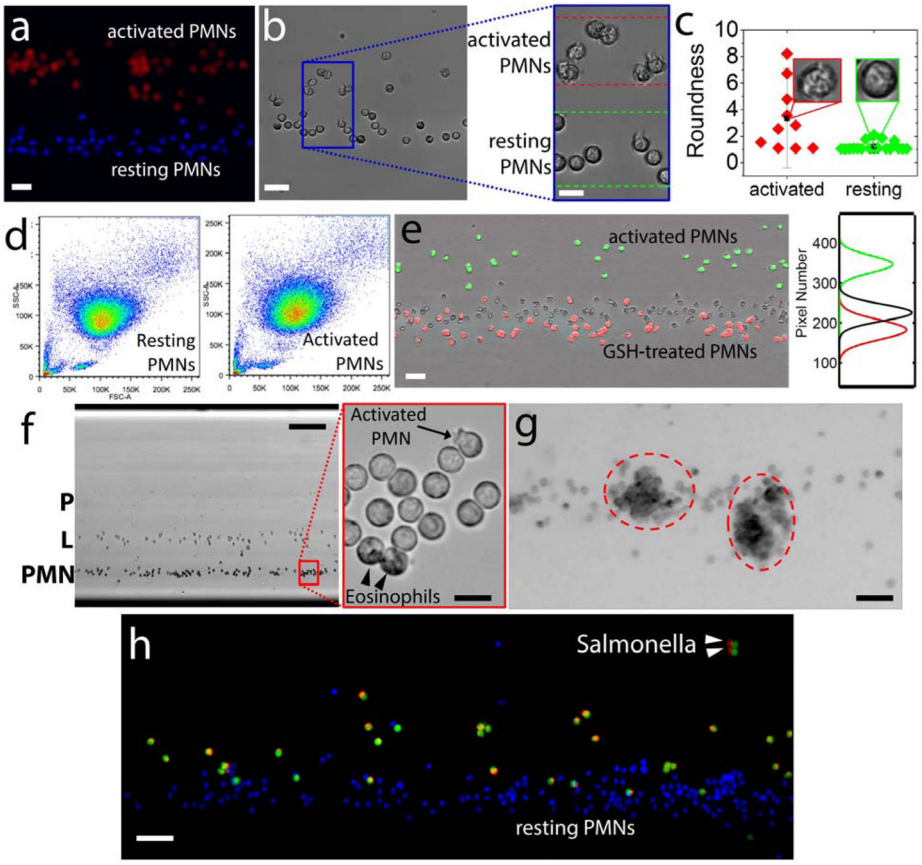

Figure 3. Static levitation of functionally-altered blood cells

(a–c) Changes in PMN density associated with PMA activation. **(a)** Low magnification, fluorescence image of magnetically focused PMNs treated with 10 nM PMA (activated PMNs, red) or buffer (resting PMNs, blue). Scale bar is 40 μm. **(b)** Low magnification, brightfield image of the levitating PMN. Scale bar is 40 μm. Inset, showing the shape and optical density differences between resting and activated PMNs. Scale bar is 20 μm. **(c)** Roundness differences between normal and activated PMNs. **(d)** Flow cytometry results for normal PMN (left) and activated PMN with PMA (right). **(e)** Scavenging intracellular ROS alters PMN confinement height. Activated PMNs (green), resting PMNs (unstained), and GSH-treated PMNs (red). Scale bar is 40 μm. **(f)** Magnetically-driven density separation of blood cells. Left panel, low magnification (4×) of buffy coat cell levitated in 30 mM Gd^{+} solution for 15 minutes, showing PMNs (PMN), lymphocytes (L) and platelets (P). Scale bar is 200 μm. Right panel, high magnification (40×) of resting PMNs, showing an activated PMNs with rough partial outline (arrow) and two eosinophils showing darker granules in the cytoplasm (arrowheads). Scale bar is 20 μm. **(g)** Low magnification (10×), two hours after levitation, PMNs underwent self-activation followed by homo-typical aggregation (red dotted circles). Scale bar is 80 μm. **(h)** Phagocytosis of salmonella by human PMNs. Resting PMNs (blue) and PMNs (green) pre-incubated with Alexa-594-labeled Salmonella were mixed, resuspended in 30 mM Gd^{+} 200 μL, and magnetically confined for 20 minutes. Arrowheads point to ingested Salmonella. Scale bar is 100 μm.

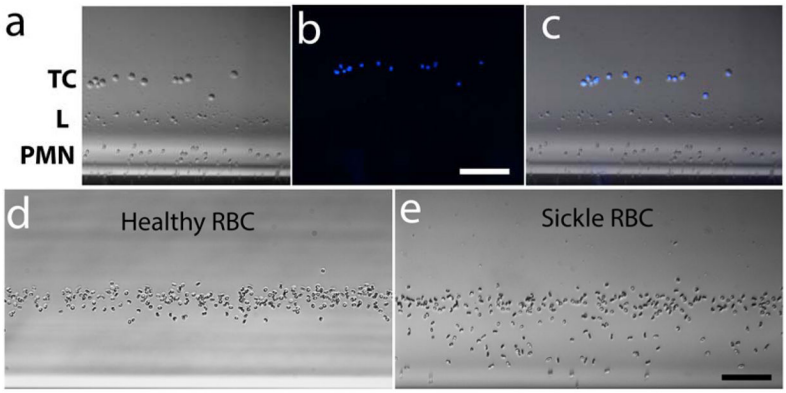

Figure 4. Versatility of magnetic levitation-based approach

(a–c) Identification of circulating tumor cells in whole blood. Diluted blood isolated from a healthy donor was spiked with breast cancer cells (TC) and magnetically confined using a low (15 mM) Gd+ concentration that allows only levitation of TC, PMNs (PMN) and lymphocytes (L) but not that of RBCs. **(a)** Brightfield image of the levitated cells. **(b)** Fluorescent image of the levitated cells. TCs are labelled with blue. **(e)** Merged image of brightfield and fluorescent image. Scale bar is 100 μm. **(d&e)** Identification of sickle cell disease by magnetic levitation. Levitation of **(d)** healthy and **(e)** sickle RBCs in the presence of 10 mM Na metabisulfite. Bright filed images of RBCs recorded after 10 minutes of confinement. Enhanced (Roberts filter), image analysis-friendly images of the same snapshots are given in Fig. S6. Scale bar is 100 μm.